

MRI of diffuse liver disease: the common and uncommon etiologies

Surya Chundru, Bobby Kalb, Hina Arif-Tiwari, Puneet Sharma, James Costello, Diego R. Martin

ABSTRACT

Diffuse liver disease, including all causes of chronic liver disease, affects tens of millions of people worldwide. There is a growing need for diagnostic evaluation as treatments become more readily available, particularly for viral liver disease. Magnetic resonance imaging (MRI) provides unique capabilities for noninvasive characterization of liver tissue that rival or surpass the diagnostic utility of liver biopsies. There has been incremental improvement in the use of standardized MRI sequences, acquired before and after administration of contrast for the evaluation of diffuse liver disease, and this includes study of the liver parenchyma and blood supply. More recent developments have led to methods for quantifying important liver metabolites, including fat and iron, and liver fibrosis, which is the hallmark for chronic liver disease. In this study, we review the MRI techniques and diagnostic features associated with common and uncommon etiologies of diffuse liver diseases, including processes that lead to abnormal perfusion (e.g. Budd-Chiari syndrome, congestive hepatomegaly), deposition diseases (e.g. fatty liver, hemochromatosis, Wilson's disease), and abnormalities that are related to inflammation and fibrosis (e.g. primary sclerosing cholangitis, sarcoidosis).

Magnetic resonance imaging (MRI) provides a better characterization of liver tissue disease processes and masses than computed tomography (CT) (1), but to achieve this relative performance, it requires attention to the details of the optimal technique. Routine MRI examination of the liver should include both single-shot T2-weighted and breath-hold T1-weighted images (2), and they should include gadolinium enhancement with the acquisition of multiple phases. The T1-weighted precontrast images must include in-phase and out-of-phase acquisitions to assess the hepatic lipid or iron content. T1-weighted pre- and postgadolinium enhanced images are acquired using a fat-suppressed three-dimensional gradient-echo (3D GRE) technique (3). These images are most commonly acquired in the axial plane with an in-plane resolution of approximately 2 mm and a 2–3 mm resolution on the z-axis. Using various acceleration techniques, including parallel processing and undersampling, 3D GRE images that cover the entire liver from the base of the lungs to below the kidneys may be acquired in under 15 s during a single breath hold. Dynamic enhanced postgadolinium images are acquired to characterize tumors and diffuse liver disease. Timing of the arterial phase images is critical for providing unique diagnostic information for determining the perfusion characteristics of hepatic lesions and revealing hemodynamic changes related to active liver disease. The venous and delayed recirculation phase images, which are sometimes referred to as the “equilibrium” phase, are used to detect other characteristic features delineating different tumor types for grading hepatic fibrosis related to chronic liver disease and for delineating vascular abnormalities such as detecting and distinguishing bland from tumor thrombus in the portal vein. In chronic liver disease, dynamic postgadolinium images are critical for the detection and characterization of regenerative or dysplastic nodules and hepatocellular carcinoma (HCC). The same sequences that are useful for liver evaluation provide a comprehensive evaluation of all of the soft tissues of the abdomen and allow the detection of most of the important diseases, facilitating the use of a universal protocol for abdominal imaging.

This review article discusses acute and chronic liver disease processes in light of the MRI features and techniques that are used for the evaluation of diffuse liver diseases, including processes that lead to abnormal lipid metabolism, iron deposition disease, and perfusion abnormalities that are related to inflammation, fibrosis, vascular occlusion or infarction, and hemorrhage.

Budd-Chiari syndrome (hepatic vein thrombosis)

The original description of Budd-Chiari syndrome was related to a severe, often fatal, acute form of hepatic vein thrombosis (4). Currently, Budd-Chiari syndrome is used to describe any form of pathology that

From the Department of Radiology and Medical Imaging (D.M. [✉ dmartin@radiology.arizona.edu](mailto:dmartin@radiology.arizona.edu)), University of Arizona College of Medicine, Tucson, Arizona, USA.

Received 16 April 2013; accepted 15 May 2013.

Published online 6 August 2013.
DOI 10.5152/dir.2013.13148

is related to hepatic venous thrombosis (4). Thrombosis within hepatic veins occurs most commonly as a result of hypercoagulable states; these occur more commonly in women and can be associated with underlying conditions, including pregnancy or postpartum states, lupus, sepsis, polycythemia, and neoplasm, particularly hepatocellular carcinoma.

In Budd-Chiari syndrome, hepatic venous outflow obstruction results in congestion and ischemia that can eventually lead to atrophy and fibrosis (4). Depending on the degree of involvement, spared segments of the liver will undergo compensatory hypertrophy. The caudate lobe characteristically has separate drainage to the inferior vena cava and is usually spared; it often undergoes hypertrophy over time. Hepatic venous drainage is variable, and other segments of the liver are also commonly spared, which leads to variable regions of hypertrophy. The characteristic liver MRI pattern of Budd-Chiari syndrome in the acute, subacute, and chronic states has been described (Fig. 1) (4). In the acute state, the central liver shows low T1-weighted and mildly elevated T2-weighted signal secondary to congestive edema with irregular increased enhancement on the arterial postgadolinium phase images. In the subacute phase, this pattern of T1-weighted and T2-weighted signal intensity and postgadolinium enhancement is seen to migrate toward the periphery of the liver. In the acute and subacute states, hepatic vein thrombosis is best visualized on postgadolinium venous or delayed phase breath-hold 3D GRE images. In the chronic phase, visualization of the hepatic vein thrombus may become less apparent. However, there may be characteristic hypertrophy of the caudate lobe that is often massive, as well as hypertrophy of other spared segments; this latter pattern is more frequent. The liver segments that are affected by chronic hepatic venous obstruction show atrophy and fibrosis. Fibrotic regions may show progressively increasing enhancement on delayed postgadolinium images, with regenerative nodules showing higher T1-weighted signal and intermediate to low T2-weighted signal, with marked enhancement on arterial-ve-

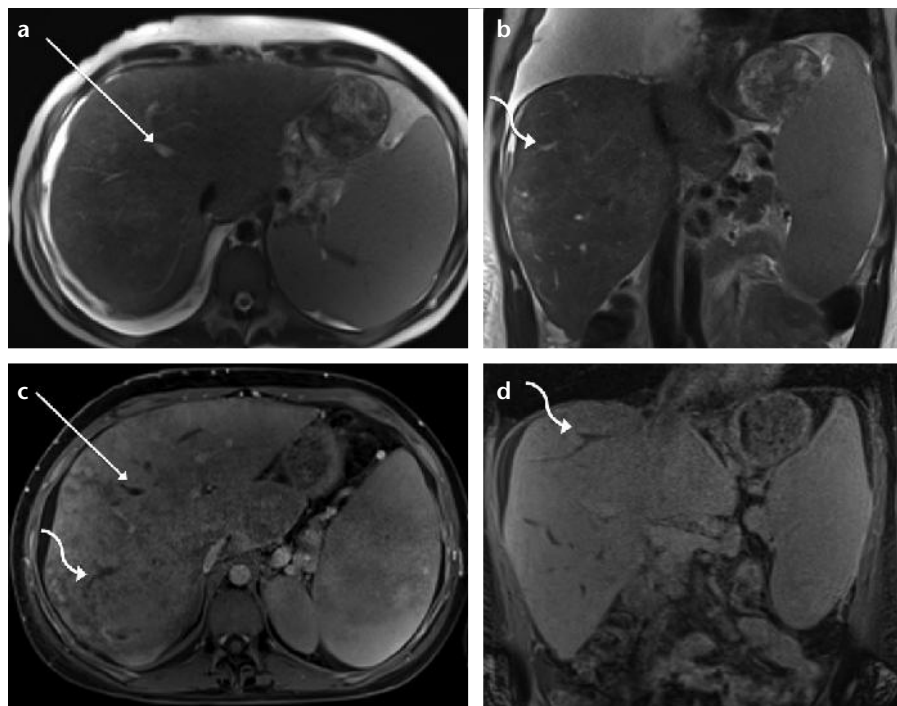


Figure 1. a–d. Budd-Chiari syndrome. T2-weighted axial (a) and coronal (b) images demonstrate abnormal signal in the middle hepatic vein (a, arrow), and right hepatic vein (b, curved arrow). T1-weighted delayed axial (c) and coronal (d) postcontrast images show a corresponding filling defect in the middle hepatic vein (c, arrow), and right hepatic vein (c, curved arrow). Likewise, there is a filling defect in the right hepatic vein on the delayed coronal image (d, curved arrow).

nous phase postgadolinium spoiled gradient-echo images.

Hepatic venous thrombosis that results from direct invasion by a tumor is most commonly related to HCC. In the case of tumor thrombosis, soft tissue enhancement on postgadolinium breath-hold 3D GRE arterial phase images is diagnostic. In addition, single-shot T2-weighted images show a characteristic elevated signal intensity within the hepatic vein, and the vein is typically distended. These features should not be observed in the setting of subacute to chronic benign thrombus. In addition, diffuse infiltrative HCC that involves the hepatic veins also commonly involves the portal veins. Infiltrative HCC characteristically develops an elevated T2 signal with relatively well-demarcated tumor margins. In contrast, Budd-Chiari syndrome may lead to an elevated T2 signal within the liver due to congestion, but there will be no demarcation of the margins.

Congestive hepatopathy

Persistent elevation in central venous pressure secondary to right-side

cardiac failure can lead to hepatic congestion with pathologic changes that appear as nutmeg liver on histology (5). In chronic cases, some patients go on to develop cirrhosis. On MRI, hepatic congestion can be diagnosed based on a constellation of findings, including cardiac enlargement, dilated hepatic veins, hepatic edema, and irregular postgadolinium hepatic enhancement on multiple phases (Fig. 2). In addition, enhancement with a fine reticular and coarse linear pattern that develops progressively on venous and delayed phase images is consistent with the development of irreversible chronic liver disease and hepatic fibrosis (5).

Toxemia of pregnancy

Uncontrolled hypertension in late third-trimester pregnancy can be associated with a syndrome that includes hemolytic anemia, elevated liver serum enzymes, and low platelets (HELLP). Liver injury is common in HELLP, and this occurs as a result of platelet abnormality and microvascular occlusions in the liver that can lead to ischemic

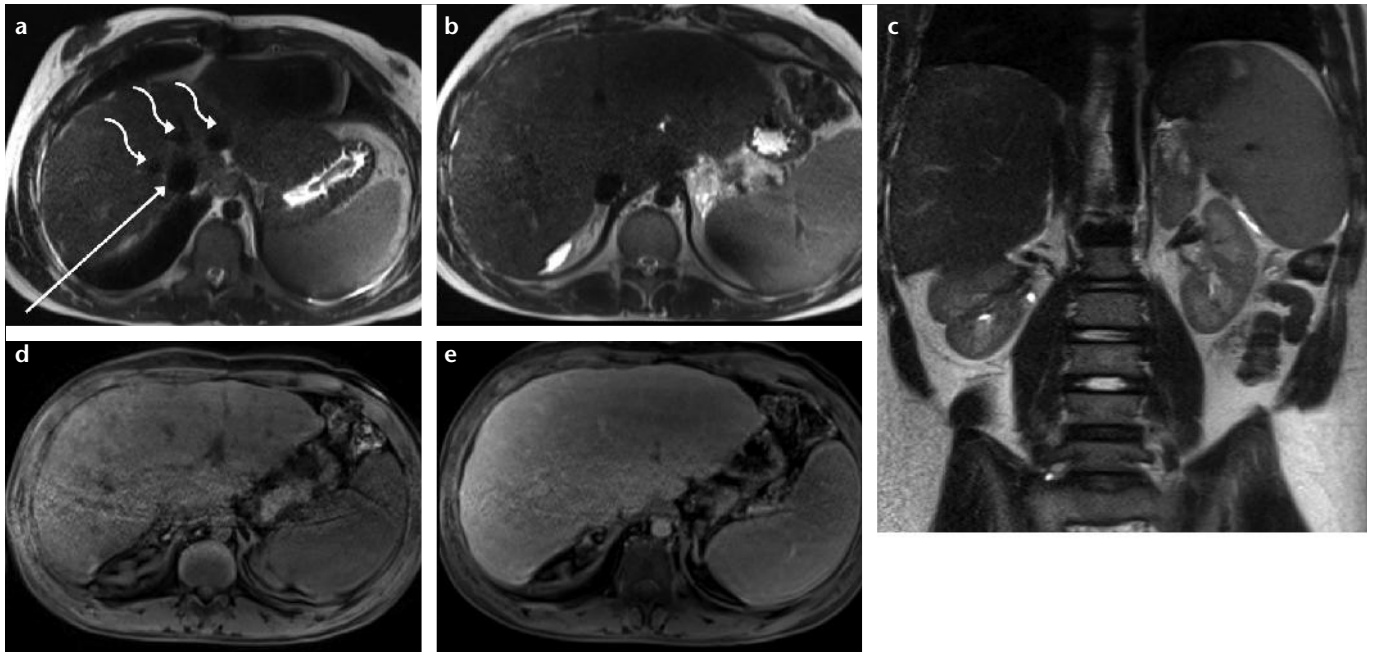


Figure 2. a–e. Congestive hepatopathy. T2-weighted axial (a, b) and coronal (c) images demonstrate that the hepatic veins (a, curved arrows) and inferior vena cava (a, arrow) are distended and appear to have large flow voids. Splenomegaly is shown on the T2-weighted coronal image (c). T1-weighted delayed postcontrast images (d, e) show that a moderately severe reticular and coarse linear peripheral subcapsular pattern of delayed enhancement is present, which is a marker of fibrosis. These are features of moderately advanced diffuse chronic liver disease, and these are sequelae of chronic congestive hepatopathy.

injury and hemorrhage. Pathologically, fibrin deposits are found in the sinusoids, with hemorrhage extending into the subendothelial space. Hemorrhage can extend along the portal triads and form small pools of blood. In more severe cases, the hemorrhage can be more extensive, and it may dissect through the hepatic parenchyma into the subcapsular space and rupture through the capsule into the free intraperitoneal space (6, 7). In severe cases, hemorrhage can be life-threatening. Precontrast MRI can show areas of irregular high and low T1-weighted and T2-weighted signal that correspond to areas of edema and blood products, and blood products produce characteristic elevated signal intensity on 3D GRE precontrast images. MRI can provide superb characterization of perfusion abnormalities on dynamic enhanced postgadolinium 3D GRE images. Active microhemorrhages appear as areas of slowly pooled accumulation of gadolinium, and blood products in fluid-filled spaces appear as fluid with irregular elevated T1-weighted and variable decreased T2-weighted signal intensity. Ultrasound has been used as a screening tool, but its sensitivity and specificity are unknown. CT imaging of liver changes in HELLP have

been reported (6, 7), but a nonionizing imaging test is clearly preferred in this young female patient population, particularly if longitudinal imaging is planned to follow the disease process to resolution.

Biliary disease: primary sclerosing cholangitis

Primary sclerosing cholangitis (PSC) is a disease of unknown etiology that is characterized by inflammation and fibrosis of the liver and the bile ducts; it is often associated with inflammatory bowel disease, and particularly ulcerative colitis (8). A good correlation between MR cholangiopancreatography (MRCP) and endoscopic retrograde cholangiopancreatography (ERCP) in diagnosing PSC has been demonstrated (8). MRCP has potential advantages over ERCP. MRCP is noninvasive and provides reliable evaluation of the smaller and more peripheral bile ducts that are frequently involved in the disease process but are not observed on ERCP. MRCP may be used to identify the group of patients who might benefit from therapeutic ERCP, and it may detect additional abnormalities such as early cholangiocarcinoma. The most common MRI findings are intrahepatic ductal irregular segmental stenosis

with intervening dilated segments, which sometimes generate a beaded appearance; the diseased segments are stenotic, and the dilated segments represent regions of relative sparing (Fig. 3) (8). The key feature of PSC is randomly distributed annular strictures that are disproportionate to upstream dilatation. With disease progression, the stricture increases and obliterates the peripheral ducts, producing a characteristic pruned appearance. Wall-thickening and enhancement of the extrahepatic bile duct are potential findings on the contrast-enhanced dynamic images, but these should raise the concern for malignancy. MR images of the liver in patients with PSC often have patchy peripheral areas of atrophy and abnormal signal intensity and enhancement with characteristic central regeneration (Fig. 4) (9). Longitudinal evaluation by MRI is warranted to monitor disease progression and to screen patients for possible development of cholangiocarcinoma (8), which these patients are at risk of developing. We have noted that HCC in these patients is extremely unlikely.

MRI in patients with PSC should include a comprehensive abdominal exam that includes T2-weighted, pre- and postcontrast enhanced 3D GRE.

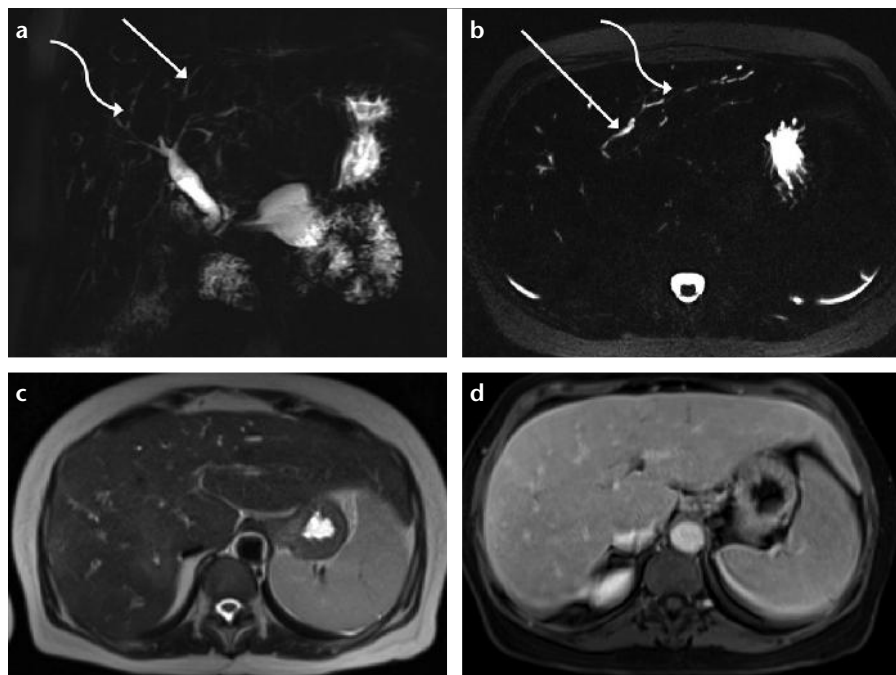


Figure 3. a–d. Primary sclerosing cholangitis at moderate stage. Coronal (a) and axial (b) MR cholangiopancreatography images reveal that there is irregular stenosis (curved arrows) with intervening dilated segments (arrows) of the intrahepatic bile ducts. Axial T2-weighted image (c) demonstrates the regional areas of increased signal in the liver. T1-weighted postcontrast axial image (d) shows increased uptake of contrast in the peripheral aspect of the anterior right hepatic lobe, showing a reticular and subcapsular coarse linear pattern with early focal confluence, which are markers of hepatic fibrosis. Note the central liver hypertrophy and relative sparing of fibrotic tissue markers.

MRCP is a historical term that refers to a more heavily T2-weighted technique, which is used to generate high contrast images of the fluid-filled structures, including the bile ducts, and displays little signal from the soft tissues. Such images may be acquired within 2–5 s using a single-shot slab in the coronal plane with 40–50 mm slice thickness. The benefits of this technique include speed, but the limitations include volume averaging with other fluid-containing structures such as a distended stomach or ascites. A 3D MRCP technique may be used to generate a dataset constructed with high resolution in three dimensions, which allows reconstruction in multiple planes. The limitations of 3D MRCP include longer acquisition time, which is in the range of several minutes, and the requirement for respiratory triggering, which reduces the reliability of this method. Generally, MRCP by any technique provides visualization of bile duct morphology, but it does not evaluate the soft tissues; the bile duct walls, the liver parenchyma or the hepatic vasculature, which is essential for complete assessment of

patients with PSC. Therefore, a complete examination of these patients warrants a comprehensive MRI study that includes conventional single-shot T2-weighted and multi-phase contrast enhanced 3D GRE.

Miscellaneous: radiation fibrosis

When a therapeutic radiation portal includes the liver within the exposure field, there is a risk of developing radiation fibrosis. The acute phase is associated with inflammation and edema, and chronic changes include fibrosis and tissue retraction. The imaging features can be characterized based on an abnormal liver signal with the distribution following well-delineated linear margins corresponding to the external radiation beam, but not following anatomic liver segments. Acute changes show an elevated signal on T2-weighted images and a low signal on T1-weighted images. Chronic changes are characteristic and show a slightly elevated signal on T2-weighted images with increased enhancement on arterial phase postgadolinium images that persists and may become more intense in the

delayed phase. This may be due to the greater susceptibility of the portal venous branches to radiation fibrosis, retraction, and occlusion, with subsequent preferential hepatic arterial supply to the involved hepatic tissue. The hepatic veins may also be affected preferentially and may result in impaired and delayed gadolinium contrast outflow. In addition, gadolinium contrast may have increased interstitial distribution in fibrotic tissues as a result of the increased tissue uptake in the setting of fibrosis. Both factors would contribute to elevated contrast concentration on delayed phase images.

Granulomatous disease: sarcoidosis

Sarcoidosis is pathognomonic described on histology as noncaseating epithelioid granulomas with surrounding fibrosis in the periportal region and portal tracts. It occasionally involves the liver, spleen, and subdiaphragmatic lymph nodes, usually after bilateral hilar adenopathy has developed. MRI findings are hepatosplenomegaly with or without numerous, usually small, hypointense T1 and T2 nodules compared to the surrounding parenchyma and that enhance on the gadolinium-enhanced 3D GRE images. Such intensities may correspond histologically to granulomas, and the spleen intrinsically generates relatively high signal intensity on T2-weighted images, which may account for the relatively lower T2-weighted signal that is generated by sarcoid nodules.

Hepatic deposition diseases

Lipid accumulation in hepatocytes can occur as a result of impaired liver function secondary to a variety of etiologies (10), which are most commonly obesity, type II diabetes and dyslipidemia. In the USA, fatty liver can be detected in more than 20% of the population; the most common association with fatty liver is obesity. Fatty liver disease covers a wide spectrum ranging from dormant noninflammatory fatty liver to hepatic steatosis with inflammation (nonalcoholic steatohepatitis) (Fig. 5), fibrosis, and eventually cirrhosis. In the setting of liver transplantation, a living related donor liver assessment must include evaluation for the presence of fatty infiltration; this is

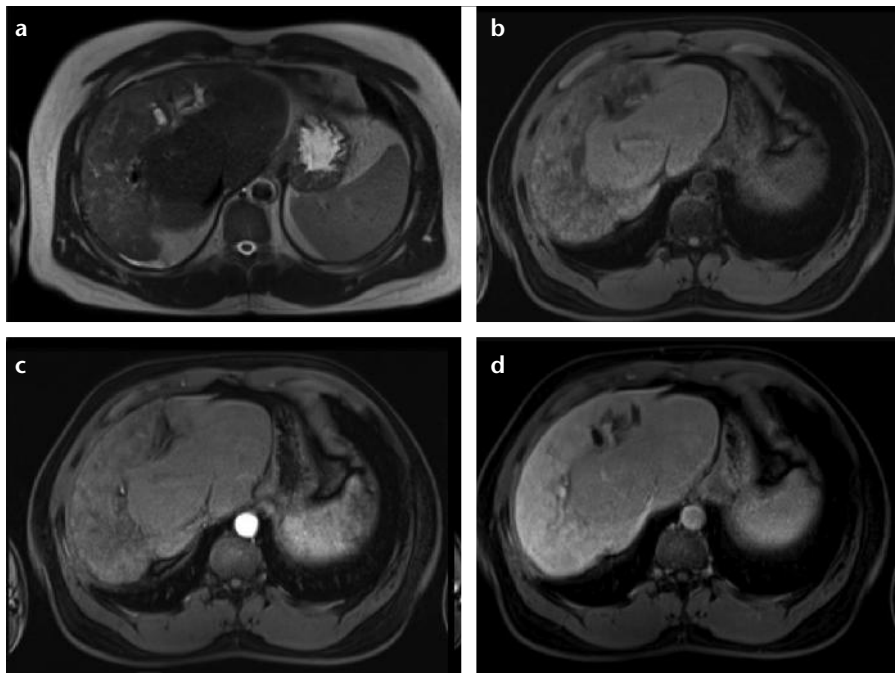


Figure 4. a–d. Primary sclerosing cholangitis at severe stage. T2-weighted axial (a), T1-weighted precontrast (b), and postcontrast (c, d) images show that the peripheral liver of all segments and of both lobes are contracted in volume relative to the central highly hypertrophied liver, comprised mostly of the caudate. This provides an excellent opportunity to visualize different stages of chronic liver disease within the same patient. While the central liver is relatively normal, the peripheral liver shows advanced fibrosis and contraction. Note that the T2 signal in the peripheral liver is higher with defined strands of elevated T2 signal, corresponding to fibrotic tissue that is best represented on the enhanced 3D gradient-echo imaging. The precontrast (b) and arterial phase (c) images show nodular tissue corresponding to regenerative nodules. These show an elevated signal compared to intervening reticular and linear pattern with low signal fibrotic tissue. This is due to higher protein content within hepatocytes, which causes an elevated T1 signal and increased vascularity, which leads to greater enhancement on arterial and venous phase images. The delayed phase image (d) shows progressive uptake and enhancement of the fibrotic tissue. Note that the fibrotic peripheral liver develops markedly increased enhancement compared to the centrally spared liver. The overall morphology and pattern of disease demonstrated in this case are characteristics of primary sclerosing cholangitis.

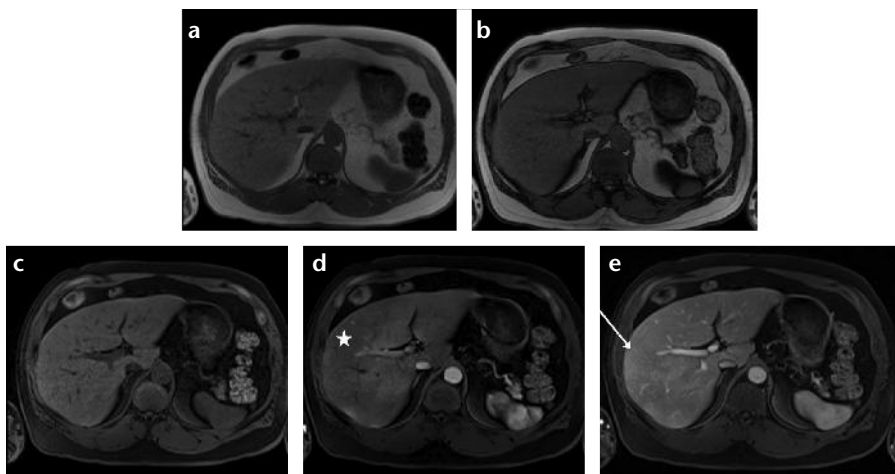


Figure 5. a–e. Steatohepatitis. Axial in-phase (a) and out-of-phase (b) images show the diffusely diminished signal intensity of the liver in the out-of-phase compared to in-phase images of liver in relation to skeletal muscle. The T1-weighted precontrast axial image (c) demonstrates normal uniform signal intensity of the liver. T1-weighted postcontrast axial images (d, e) show abnormal heterogeneous enhancement (*star*) in the arterial phase (d). There is also abnormal enhancement that has developed on the delayed phase postcontrast 3D gradient-echo T1-weighted image (e) along the subcapsular anterior right lobe with a thin linear and fine reticular pattern (*arrow*), which is a marker of regionally advanced fibrosis. This is the most common location for the earliest development of hepatic fibrosis related to chronic liver disease. In this case, the overall findings are suggestive for nonalcoholic fatty liver disease that is progressing to nonalcoholic steatohepatitis.

considered a contraindication to transplantation when severe and can lead to failure of the transplant (11). Abnormal lipid accumulation in the liver can be detected on MRI (12, 13) and can be evaluated on the basis of comparing the liver signal on spoiled gradient-echo images that are acquired in-phase and out-of-phase (14). Hydrogen protons in a voxel that contains 100% fat will precess 220 to 230 Hz slower than a voxel that is made up of 100% water at 1.5 Tesla. That means that every 4.4 ms, most of the fat protons will migrate 360° and regain in-phase orientation relative to water protons, whereas at 2.2 ms, or at half this time, the fat and water protons will be 180° out-of-phase. Current generation MR systems have incorporated dual-echo breath-hold spoiled gradient-echo sequences that can acquire two sets of filled k-space generating two sets of images; one set is out-of-phase and the other in-phase with all other parameters identical, including spatial registration. These acquisitions are available as two-dimensional or 3D multiple gradient-echo sequences. Liver containing hepatocytes with intracellular lipid result in image voxels with a physical mixture of water and lipid, which when imaged out-of-phase, results in phase cancellation and diminished signal (Fig. 6). Automated spectroscopic methods allow for reproducible and accurate quantification of the total lipid content. The spleen does not accumulate fat and can therefore be used as a control against which the liver signal can be assessed as a ratio to test for relative diminishment of the liver signal on out-of-phase images. The spleen signal can change as a result of iron deposition, and the use of kidney or skeletal muscle within the image may be more reliable for the assessment of relative liver signal changes between in-phase and out-of-phase images. Fat accumulation in the liver can be diffuse, diffuse with focal sparing, or focal (Fig. 7). Focal fatty accumulation typically occurs around the falciform ligament, gallbladder fossa, and the inferior vena cava (15). One possible explanation is that these areas of the liver are prone to irritation or stimulation, which results in local changes in carbohydrate-lipid metabolism. Contrast-enhanced

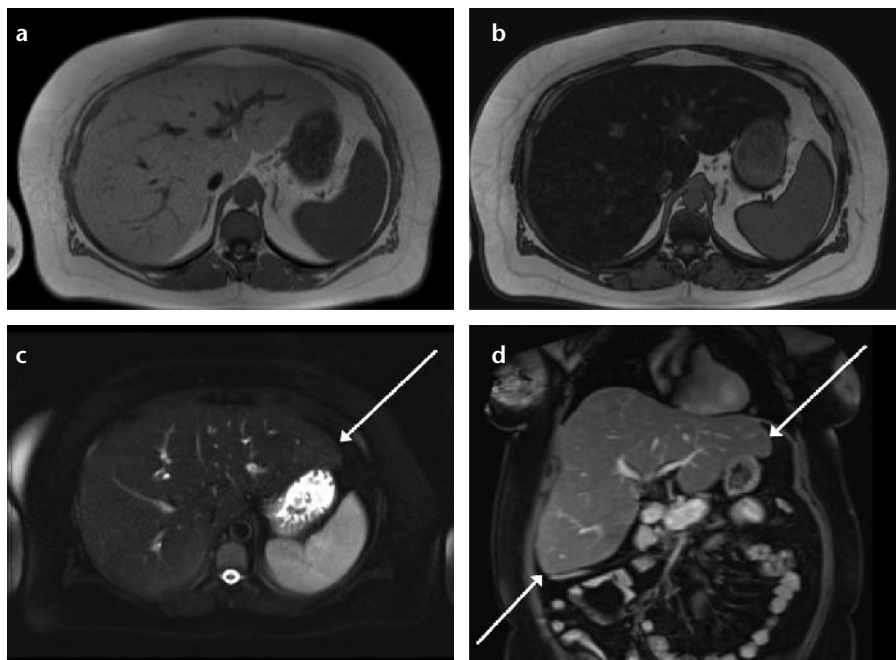


Figure 6. a–d. Hepatic steatosis. Axial in-phase (a) and out-of-phase (b) images show the diffusely diminished signal intensity of the liver on the out of-phase compared to the in-phase images, which is indicative of hepatic steatosis. It is optimal to compare these against skeletal muscle, which should not show appreciable changes in lipid or iron levels, and serve as an internal reference for changes occurring in the liver signal. The T2-weighted fat-saturated axial (c) and T1-weighted delayed postcontrast coronal (d) images show otherwise normal liver with no other changes of chronic liver disease, namely changes of hepatic fibrosis or portal hypertension. Note that the liver edges are rounded (arrows) as a result of hepatomegaly.

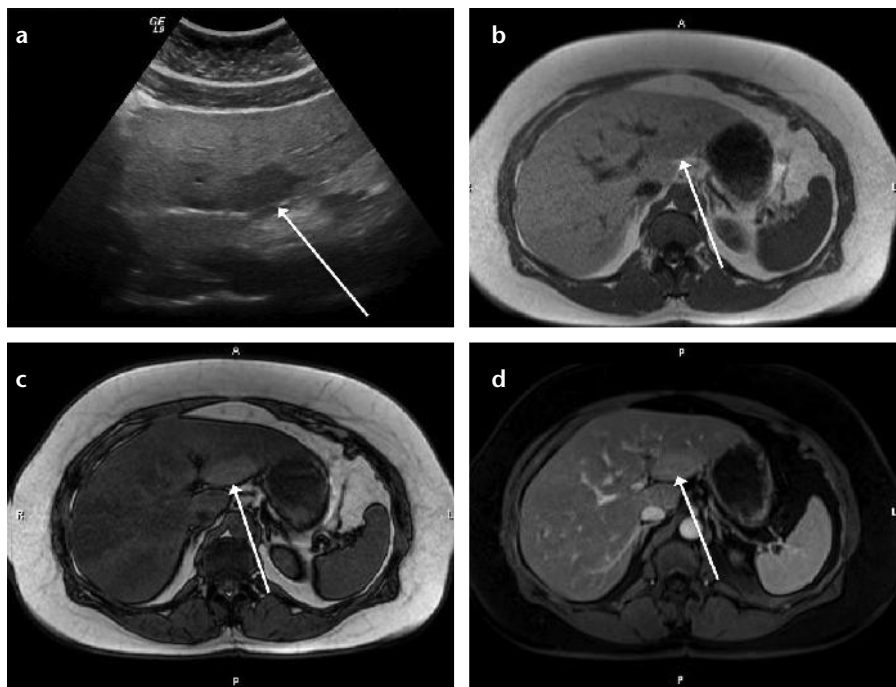


Figure 7. a–d. Focal fat sparing. The axial ultrasound image (a) shows a hypoechoic area (arrow) in the left hepatic lobe. Axial in-phase (b) and out-of-phase (c) images show that the liver diffusely diminishes in signal intensity on the out-of-phase compared to the in-phase images. An exception is noted in the posterior aspect of segment III (b, c, arrows) of the left hepatic lobe, which precisely corresponds to the lesion on the ultrasound. This focus shows no appreciable drop in signal on the out-of-phase image, while also showing mildly diminished signal on the in-phase image; the elevated lipid fraction in the surrounding liver generates greater T1 signal intensity, creating the appearance of a low signal intensity nodule on the in-phase image. The focus of focal fatty sparing appears to be more greatly enhanced in the adjacent liver (d, arrow). However, this is due to the fat-suppression technique used with the 3D gradient-echo sequence (d), which lowers the signal of the liver that surrounds the fat-spared nodule.

CT and standard ultrasonography are nonspecific and less sensitive for the assessment of fatty liver and can confuse irregularly accumulated lipid with a mass (Fig. 7). Diffusely fatty liver can lead to reduced CT density and can diminish contrast between a low-density mass and the adjacent liver, which may make the mass less conspicuous.

More recent technical developments have yielded both MRI and MR spectroscopy tools for rapid, accurate and reproducible quantification of the hepatic lipid fraction (12). These tools will become increasingly available on commercial MR systems for routine clinical application.

Hemochromatosis

Iron can accumulate within the liver through two basic mechanisms: accumulation within hepatocytes through normal metabolic chelation mechanisms or uptake within the phagocytic Kupffer cells, which represent part of the reticuloendothelial system (16). Serum iron and transferrin saturation are poorly correlated with the degree of iron overload. Although serum ferritin can be used to estimate body iron stores, a variety of etiologies can lead to elevation of serum levels independent of total body iron.

In primary hemochromatosis, the defect seems to be due to the combination of inappropriately regulated small bowel that leads to increased uptake of dietary iron, which results in excess total body iron accumulation (16), and the inappropriate cellular regulation of intracellular iron within hepatocytes. Hepatocytes chelate the iron that accumulates within the cytosol. The pancreas also has chelation mechanisms within the acinar cells that can accumulate excess intracellular iron (17); however, to some degree, iron accumulation can occur in most tissues, typically as a late feature that occurs after hepatic stores have reached high levels. Important examples include the pituitary and heart, where this can result in impaired pituitary function, fatal cardiac arrhythmias, or congestive heart failure (17). Patients who present with a first-time diagnosis of primary hemochromatosis with the combined findings of elevated liver and cardiac iron deposition, and congestive heart

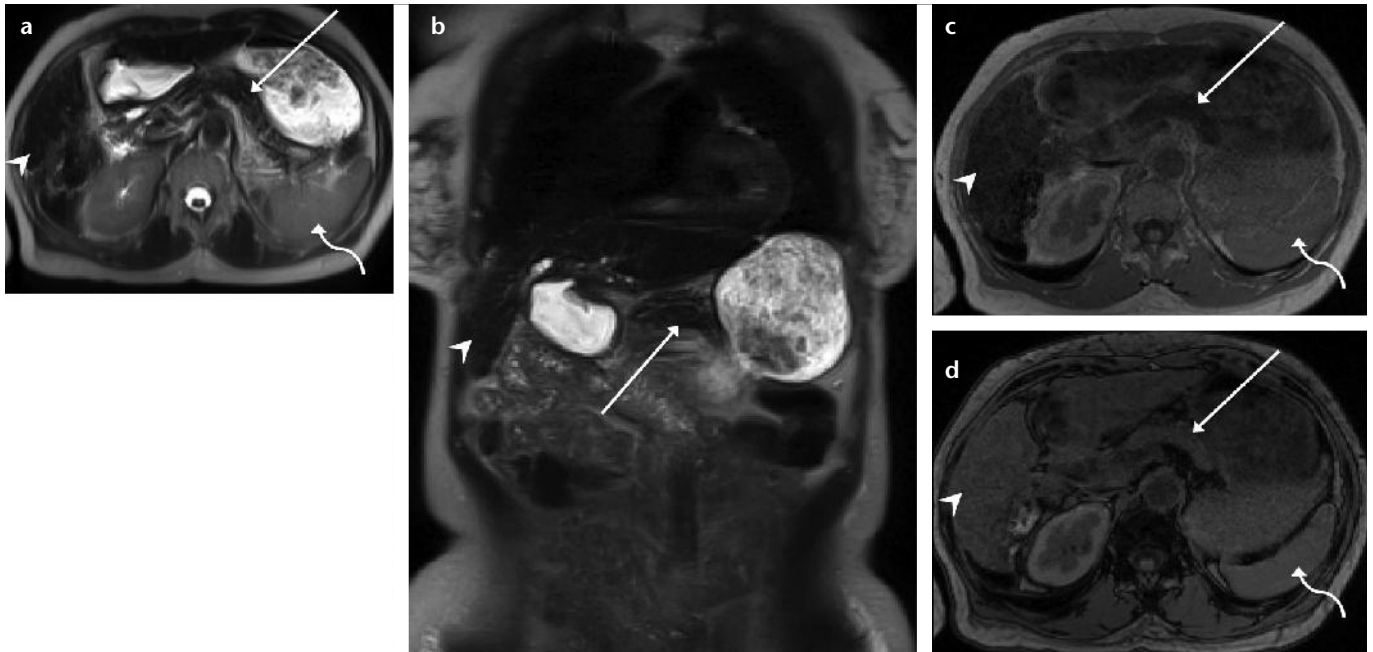


Figure 8. a–d. Primary hemochromatosis. T2-weighted axial (a) and coronal (b) images show that there is low signal in the liver (arrowheads) and pancreas (arrows), which is conspicuous on the T2-weighted images characteristic of tissue iron accumulation; the liver should normally develop a similar signal to the pancreas but with higher signal intensity than skeletal muscle. In this case, the liver has lower signal intensity compared to skeletal muscle. Axial in-phase (c) and out-of-phase (d) images confirm this through the noted loss of liver and pancreas signal intensity on the in-phase compared to out-of-phase images (arrows and arrowheads). Note that the spleen (a, c, d, curved arrows) shows normal signal intensity on T2 and shows no signal changes between the in-phase and out-of-phase images.

failure have a poor prognosis with a six-month life expectancy. There has been rapid development of the understanding of the genetic basis of this disease, which consists of a defective hemochromatosis gene. The defective hemochromatosis gene seems to represent the most common inherited genetic disease among people of European descent; it occurs in 1 in 40 Americans and has a 1 in 400 incidence of homozygosity. The phenotypic expression of this disease is more complicated, however, and seems to follow a polygenetic penetrance pattern. An inexpensive and clinically available genetic test may be used for targeted screening purposes.

In secondary hemochromatosis, iron overload can occur secondary to excess red cell turnover from exogenously derived red cells as a result of blood transfusion therapy; this is observed in patients who have underlying red cell or bone marrow abnormalities, such as thalassemia, mastocytosis, or myelofibrosis. Alternatively, endogenously derived excess iron from red cell turnover can result from polycythemia rubra vera, from myoglobin in rhabdomyolysis or from siderosis that is related to al-

coholic liver disease (16). In secondary hemochromatosis, the mechanism of iron accumulation is different than in primary hemochromatosis. It results from increased uptake of iron that is derived from dying or abnormal red cells taken up by the reticuloendothelial system; this leads to iron accumulation in the Kupffer cells within liver sinusoids. Similarly, the splenic phagocytic reticuloendothelial system will engulf abnormal red cells and actively accumulate iron from hemoglobin. In contrast to primary hemochromatosis, the pancreas typically does not accumulate iron (17).

The additional clinical significance of hemochromatosis includes the observation that many patients develop cirrhosis, and approximately 25% of patients will develop HCC. MRI of the liver also can evaluate these processes. This is a phenomenon of hemochromatosis but not of secondary hemochromatosis. Furthermore, we have noted that the most common cause of abnormal secondary hepatosplenic accumulation of iron is observed in patients taking oral iron supplements, usually as part of chronic renal insufficiency.

Liver biopsies have been used for biochemical determination of liver iron overload and have been used as the basis for therapy management in patients who are treated by periodic phlebotomy and iron chelation therapy; however, this method has bleeding risks associated with the invasive procedure, and it is also susceptible to sampling error in patients who have heterogeneous iron deposition in the liver. The sensitivity of CT is insufficient, as there is a minimum threshold for liver iron detection that is more than five times greater than the normal liver iron level.

MRI is sensitive to iron concentration in the liver because of the paramagnetic properties of iron. This results in T2 or T2* effects that diminish the signal intensity on single-shot T2 images (Fig. 8) and on breath-hold T1-weighted multiecho spoiled gradient-echo images (18). Historically, we have used visual inspection of the images acquired as part of a comprehensive abdominal MRI for the qualitative or semi-quantitative evaluation of hepatic iron levels. Coronal breath-hold T2-weighted single-shot fast spin-echo images, which should be obtained as part of a routine abdominal

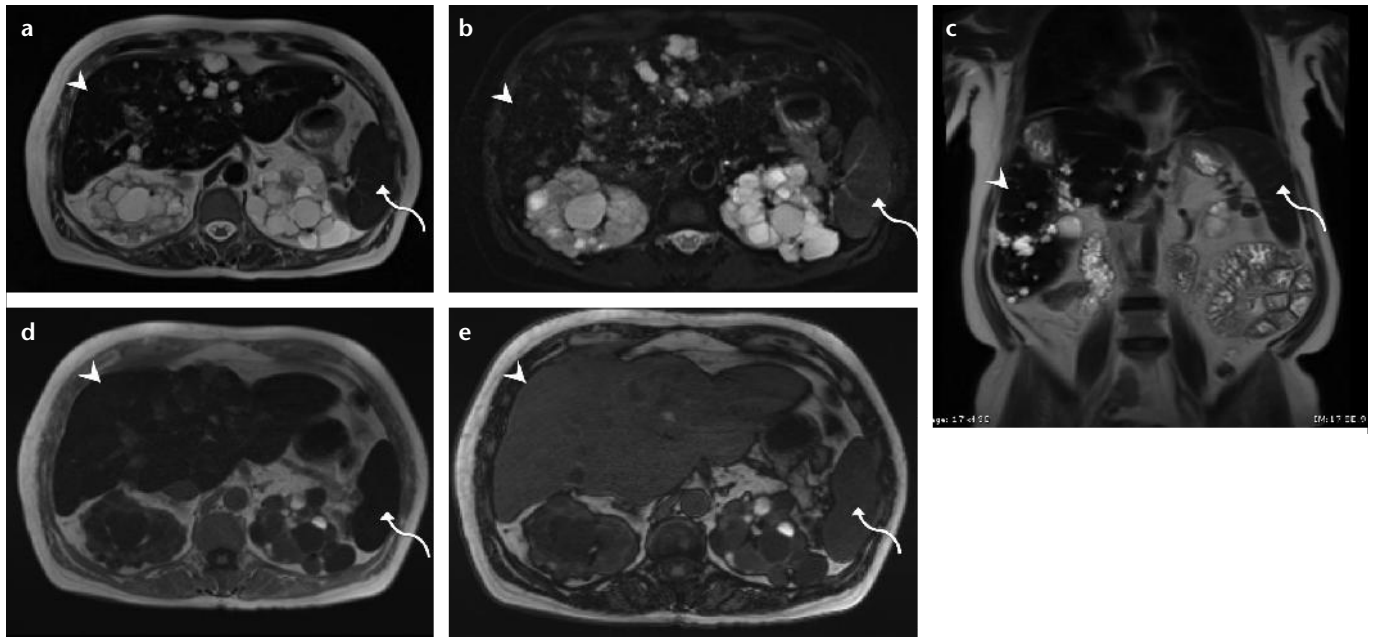


Figure 9. a–e. Secondary hemochromatosis. The liver (*arrowheads*) and spleen (*curved arrows*) show diminished signal compared to skeletal muscle on the T2-weighted images (**a–c**), which is a marker of iron accumulation. This is confirmed by the noted lower signal intensity of the liver and spleen on the longer echo in-phase image (**d**) compared to the shorter echo out-of-phase image (**e**) (*arrowheads* and *arrows*). However, the hepatosplenic pattern of iron uptake is common, and it is commonly associated with chronic kidney disease and increased oral iron supplement intake. It is also not found to be associated with impaired liver function or chronic liver disease risk. The pancreas has normal signal intensity (not shown).

MRI examination, are useful for rapid visual evaluation because they provide slices that include liver, psoas muscle, and spleen within the same image. Normally, liver signal intensity is near the midpoint in between the lower signal intensity of muscle and the higher signal intensity of spleen. In iron overload disease, the liver signal intensity becomes as low or lower than skeletal muscle. In secondary iron overload, the spleen similarly becomes dark (Fig. 9). In cases in which there is a bone marrow abnormality, such as in myelofibrosis, normal high signal marrow fat becomes replaced with low signal cellular marrow hypertrophy and sclerosis. Generally, the T2* decay rate is more sensitive to lower levels of intracellular iron accumulation. Intracellular iron accumulation can cause localized magnetic field distortion that leads to susceptibility effects that result in more rapid loss of phase-dependent signal. Routine imaging of the abdomen and liver should include a dual-echo spoiled gradient-echo acquisition that can be used in conjunction with the coronal single-shot T2. The longer echo image (TE, 4.4 ms) should show darkening of the liver compared with the shorter echo image (TE, 2.2 ms) in the setting of elevated liver

iron concentration. The sensitivity to liver iron may be increased on spoiled gradient-echo imaging by increasing the TE to include, for example, echoes at 8.8 ms and 13.2 ms. If only routine shortest possible dual echo out-of-phase (TE, 2.2 ms) and in-phase (TE, 4.4 ms) imaging is used, the relative sensitivity of the single-shot spin-echo technique is more sensitive. With this approach, demonstration of low liver signal on single-shot spin-echo alone would indicate a lower liver iron concentration; demonstration of low liver signal on single-shot spin-echo and on the longer echo dual echo spoiled gradient-echo indicate higher liver iron burden. In practice, a routine qualitative multi-echo gradient-echo is not performed, and newer, more highly developed approaches are becoming available.

In current development are two fundamental approaches with well-validated results for the accurate and reproducible quantification of hepatic iron (13, 19). These methods utilize either MRI with T2* or T2 decay or MR spectroscopy, such as the HISTO technique. The HISTO technique also provides methodology for concurrent measurement of the tissue fat fraction. Centers with current MRI/MR spectroscopy

capabilities should routinely provide noninvasive longitudinal quantitative evaluation of hepatic iron levels to guide therapy for hemochromatosis.

Other deposition diseases

Wilson's disease is an autosomal recessive genetic disorder characterized by increased intestinal uptake of "free" copper, resulting in the accumulation of toxic levels of copper in the liver, brain, and cornea. Copper deposition resulting from Wilson's disease occurs in the periportal regions and along the hepatic sinusoids, which may induce an inflammatory reaction that can lead to cirrhosis. Copper has no appreciable paramagnetic effect on MRI because copper in hepatocytes may combine with proteins and remain in a dissolved uniform state within the aqueous phase of the cell cytoplasm. This disease is indistinguishable from other causes of chronic liver disease by current imaging modalities.

All known variants of identified glycogen storage diseases are inherited autosomal-recessive disorders and are characterized by the absence or deficiency of one of the enzymes responsible for producing or metabolizing glycogen. Different subtypes of glyco-

gen storage diseases involve the liver, musculature, hematopoietic system, myocardium, and kidneys. Different subtypes have varying potential for the development of chronic liver disease and hepatocellular malignancy.

Conclusion

MRI provides a comprehensive evaluation of common and important causes of diffuse liver disease, including pathologies affecting the bile ducts and liver vasculature.

Conflict of interest disclosure

The authors declared no conflicts of interest.

References

1. Semelka RC, Martin DR, Balci C, Lance T, et al. Focal liver lesions: comparison of dual-phase CT and multisequence multiplanar MR imaging including dynamic gadolinium enhancement. *J Magn Reson Imaging* 2001; 13:397–401.
2. Naganawa S, Jenner G, Cooper TG, Potchen EJ, Ishigaki T. Rapid MR imaging of the liver: comparison of twelve techniques for single breath-hold whole volume acquisition. *Radiat Med* 1994; 12:255–261.
3. Rofsky NM, Lee VS, Laub G, et al. Abdominal MR imaging with a volumetric interpolated breath-hold examination. *Radiology* 1999; 212:876–884.
4. Noone TC, Semelka RC, Siegelman ES, et al. Budd-Chiari syndrome: spectrum of appearances of acute, subacute, and chronic disease with magnetic resonance imaging. *J Magn Reson Imaging* 2000; 11:44–50.
5. Myers R, Cerini R, Lee S, et al. Cardiac hepatopathy: clinical, hemodynamic, and histologic characteristics and correlations. *Hepatology* 2003; 37:393–400.
6. Rooholamini SA, Au AH, Hansen GC, et al. Imaging of pregnancy-related complications. *Radiographics* 1993; 13:753–770.
7. Zissin R, Yaffe D, Fejgin M, Olsfanger D, Shapiro-Feinberg M. Hepatic infarction in preeclampsia as part of the HELLP syndrome: CT appearance. *Abdom Imaging* 1999; 24:594–596.
8. Vitellas KM, Keogan MT, Freed KS, et al. Radiologic manifestations of sclerosing cholangitis with emphasis on MR cholangiopancreatography. *Radiographics* 2000; 4:959–575.
9. Bader TR, Beavers KL, Semelka RC. MR imaging features of primary sclerosing cholangitis: patterns of cirrhosis in relationship to clinical severity of disease. *Radiology* 2003; 226:675–685.
10. Siegelman ES. MR imaging of diffuse liver disease. Hepatic fat and iron. *Magn Reson Imaging Clin N Am* 1997; 5:347–365.
11. Pope C, Gore J, Sostman D, Lange R, Riely C. Diffuse fatty infiltration of the liver by magnetic resonance. *Magn Reson Imaging* 1986; 4:267–270.
12. Pineda N, Sharma P, Martin DR, et al. Measurement of hepatic lipid: high-speed T2-corrected multiecho acquisition at 1H MR spectroscopy—a rapid and accurate technique. *Radiology* 2009; 252:568–576.
13. Sharma P, Martin DR, Pineda N, et al. Quantitative analysis of T2-correction in single-voxel magnetic resonance spectroscopy of hepatic lipid fraction. *J Magn Reson Imaging* 2009; 29:629–635.
14. Rofsky NM, Weinreb JC, Ambrosino MM, Safir J, Krinsky G. Comparison between in-phase and opposed-phase T1-weighted breath-hold FLASH sequences for hepatic imaging. *J Comput Assist Tomogr* 1996; 20:230–235.
15. Kier R, Mason BJ. Water-suppressed MR imaging of focal fatty infiltration of the liver. *Radiology* 1997; 203:575–587.
16. Siegelman ES, Mitchell DG, Semelka RC. Abdominal iron deposition: metabolism, MR findings, and clinical importance. *Radiology* 1996; 199:13–22.
17. Thomsen C, Wiggers P, Ring-Larsen H, et al. Identification of patients with hereditary haemochromatosis by magnetic resonance imaging and spectroscopic relaxation time measurements. *Magn Reson Imaging* 1992; 10:867–879.
18. Mitchell DG. Chemical shift magnetic resonance imaging: applications in the abdomen and pelvis. *Top Magn Reson Imaging* 1992; 4:46–63.
19. Alustiza JM, Artetxe J, Castiella A, et al. MR quantification of hepatic iron concentration. *Radiology* 2004; 230:479–484.